Electrochimica Acta xxx (2014) xxx–xxx

Contents lists available at ScienceDirect

Electrochimica Acta

journal homepage: www.elsevier.com/locate/electacta

Hydrogen evolution assisted electrodeposition of porous Cu-Ni alloy electrodes and their use for nitrate reduction in alkali

Luca Mattarozzi [1], Sandro Cattarin [*,1], Nicola Comisso [1], Arianna Gambirasi, Paolo Guerriero, Marco Musiani [1], Lourdes Vázquez-Gómez [1], Enrico Verlato [1]

Istituto per l'Energetica e le Interfasi (IENI)-CNR, C.so Stati Uniti 4, 35127 Padova, Italy

ARTICLE INFO

Article history:
Received 27 November 2013
Received in revised form 7 April 2014
Accepted 7 April 2014
Available online xxx

Keywords:
Templated Electrodeposition
Bubble Template
Porous Alloy
Electrocatalysis
Nitrate

ABSTRACT

Porous Cu-Ni alloys with a wide range of compositions have been deposited from citrate baths containing the two metal ions, under application of large current densities (-3 A cm^{-2}) leading to vigorous hydrogen evolution. The deposited alloy layers show macroscopic porosity and a spongy material made of a network of tiny dendrites. Porous RDEs reveal a significant current increase – as compared to ordinary polished electrodes – in the fast ferrocyanide reduction under pure mass transport control. Voltammograms of nitrate reduction in alkali at porous RDEs show at all potentials larger currents in comparison with experiments at compact electrodes of same composition. Electrolyses at porous sheet electrodes show large stable currents, leading to fast and selective nitrate reduction to ammonia.

1. Introduction

Templated electrodeposition is a promising method for the preparation of porous conductive structures [1], with potential applications as electrode materials in fields like electroanalysis, energy conversion and wastewater treatment. The method uses a number of templates, with a built-in porosity like the membranes of track-etched polycarbonate [2–4] and anodic alumina [5,6], or with a porosity resulting from assembly of micro- and submicro-objects like the layers of packed microspheres made of polystyrene [7,8] or silica [9,10]. Electrodeposition of metals or other conductors in the interstices provides an accurate inverse replica of the mould, and after template removal (by burning or dissolution in suitable media, in most cases hazardous) a spongy material is obtained, with an inner porosity of defined shape, size and organization.

Despite the great modellistic value, the mentioned procedures are complex, costly and time consuming, and may not be suitable for the scaling up. Moreover, in all applications in which the current is controlled by diffusion of a reacting species, only a macroporosity with typical dimension in the range of tens of microns appears useful to enhance transport, whereas a submicron porosity will not improve significantly electrode performances [9].

An alternative simple approach to preparation of macroporous layers over a large area is the deposition of metals from aqueous solutions under high cathodic currents, resulting in vigorous hydrogen evolution: in this regime, indicated in literature as "hydrogen bubble dynamic template deposition" [11], the gas bubbles act as a faint template shaping the deposit morphology and disappearing upon current interruption, so that no template removal is required and preparation occurs in a single step. An additional important advantage of this method is that, unlike those based on solid templates, it may permit formation of porous layers on substrates of complex macroscopic morphology, including e.g. grids. Several porous metals have been deposited with this approach, including Cu [11–15], Sn [12], Ni [16–19], Co [20], Ag [21,22] and Au [23] but very few alloys that are, to the best of our knowledge, all Cu-based [24–27]. Among them, porous Cu-Ni has been deposited [26] in order to prepare a nanoporous Ni/NiO foam by selective electrodissolution of Cu, but the alloy itself was not tested in electrochemical applications.

Cu, Ni and some of their alloys with noble and non-noble metals are materials of choice for electroreduction of nitrogen oxyanions [28–38]. The good activity of Cu-Ni alloys in performing NO_3^- reduction has been ascribed [33] to some sort of synergistic mechanism in which Cu sites perform an efficient adsorption of NO_3^-, and Ni sites an efficient adsorption of H-atoms resulting from discharge of H^+/H_2O. The reduction mechanism would proceed by transfer of H_{ads} to the O-moieties of the oxyanion and elimination of hydroxyl ions, with an overall activity enhancement in comparison with the

* Corresponding author.
E-mail address: s.cattarin@ieni.cnr.it (S. Cattarin).
[1] ISE Member.

http://dx.doi.org/10.1016/j.electacta.2014.04.048
0013-4686/

Table 1
Compositions of deposition baths and of the resulting porous Cu-Ni alloys (estimated by EDS).

Bath	Bath composition:0.3 M Na citrate, 1 M $(NH_4)_2SO_4$ and	Composition in at%, alloy deposited on Nb RDEs (2500 min^{-1})	Composition in at%, alloy deposited on Nb sheets (stirred solutions)
I	0.05 M $CuSO_4$, 0.25 M $NiSO_4$	$Cu_{33}Ni_{67}$	$Cu_{25}Ni_{75}$
II	0.08 M $CuSO_4$, 0.175 M $NiSO_4$	$Cu_{52}Ni_{48}$	$Cu_{44}Ni_{56}$
III	0.125 M $CuSO_4$, 0.125 M $NiSO_4$	$Cu_{70}Ni_{30}$	$Cu_{66}Ni_{34}$
IV	0.175 M $CuSO_4$, 0.10 M $NiSO_4$	$Cu_{84}Ni_{16}$	$Cu_{82}Ni_{18}$

single metals. Porous Cu-Ni electrodes may display even better performances, as indicated by preliminary evidence [39]. In this paper, we report thoroughly on deposition and characterisation of porous Cu-Ni materials, and present comparative tests of nitrate reduction in alkali at compact and porous electrodes, showing the superior performances of the latter.

2. Experimental

2.1. Materials and electrochemical equipment

The cell used for depositions was a single compartment cell, equipped with a Pt wire counter electrode wound as a spiral (total estimated surface of ca. 15 cm^2) and fixed to the inner cell wall. The solutions were prepared from deionized water (by a Millipore Elix3 system, resistivity $\rho > 15\ M\Omega\ cm$) and high purity chemicals (Sigma-Aldrich, puriss. p.a. ACS reagents). RDE electrodes were made of Cu rods (Goodfellow, 99.999% purity, diameter 0.635 cm, section area 0.317 cm^2) or Nb rods (Goodfellow, 99.9% purity, diameter 0.56 cm, section area 0.247 cm^2), inserted in a PTFE sheath and mounted on a EDI 101 rotating unit (Radiometer). Nb electrodes were used for samples devoted to EDS analyses (see below) to exclude interference from the substrate. Cathodes for prolonged electrolyses were obtained depositing alloy layers on both faces of Nb sheets (Goodfellow, 99.5% purity) or Cu sheets (Goodfellow 99.9% purity) over a surface of 10 mm x 15 mm (for a total surface of about 3 cm^2). No significant difference was observed between the layers deposited on the two metals, presumably because the substrates are rapidly covered in the initial stages of alloy deposition and most of the layer growth occurs under essentially identical conditions. Prior to deposition, electrodes were abraded with emery paper 1000 grit, rinsed in a water ultrasound bath for 15 minutes and dried in air. All data concerning current densities, deposition charge and impedance measurements are referred to geometric area.

Electrodeposition experiments were performed at $T = 22\ ^\circ C$, under potentiostatic or galvanostatic control, using an Autolab PGSTAT 302 N, equipped with a booster providing currents as high as 10 A. In potentiostatic experiments, a (Hg/HgO/1 M KOH) was used as reference electrode and all potentials are referred accordingly in text and figures. EIS measurements were taken with a Solartron 1286 Electrochemical interface and a Solartron 1254 FRA, both controlled by a ZPlot-ZView commercial software, covering the frequency range 10 kHz to 0.01 Hz with 8 points per decade. The electrode was polarized at the applied potential $E = -0.70$ V, where the electrode is blocking, to avoid any significant faradaic reaction; the potential modulation was 10 mV rms, checked to be low enough to ensure linear response.

2.2. Alloy deposition and characterization

Ordinary deposits, referred to in the following as "compact", were obtained potentiostatically (8 C cm^{-2}) from a citrate bath containing 0.7 M $NiSO_4$, 20 mM $CuSO_4$ and 0.26 M trisodium citrate, pH 6.0, according to a procedure reported in detail elsewhere [38]. Film thickness could be estimated around 2.8 μm assuming a current efficiency of 100% - actually verified only for compositions with Cu ≥ 60 at% [38]. For comparative EIS investigations a few compact electrodes were mirror polished with 0.3 μm alumina and washed in a water ultrasonic bath; they will be referred to as "compact polished". Deposition of spongy electrodes, referred to as "porous", was performed either on RDEs rotated at 2500 min^{-1}, or on sheet electrodes while keeping the solutions agitated by a magnetic stirrer. Alloy layers of suitable morphology were obtained at a current density of -3.0 A cm^{-2} from baths I-IV (pH 4.1 - 4.5) described in Table 1.

Alloy compositions in at%, estimated by EDS analysis and indicated as Cu_xNi_{100-x}, depended on stirring conditions, and higher Cu contents were obtained for deposition on RDEs than on sheet electrodes. SEM images were obtained with a FEI Quanta 200 FEG ESEM instrument, equipped with a field emission gun, operating at an accelerating voltage variable in the range of 20-30 kV. EDS analyses were performed on Nb substrates using an EDAX Genesis energy-dispersive X-ray spectrometer at an accelerating voltage of 25 kV. EDS data obtained from spongy samples are normally questionable, but appear reliable in the present case considering that the material consists only of Cu and Ni, two elements with peaks close in energy. Electron backscatter diffraction (EBSD) investigations were performed as reported elsewhere [4].

2.3. Electrochemical tests in cathodic reactions.

Ferricyanide reduction was studied with polished Au and porous Cu-Ni RDEs in deaerated solutions containing 20 mM $K_3Fe(CN)_6$, 20 mM $K_4Fe(CN)_6$ and 1 M KOH. Experiments of nitrate reduction were performed in a two-compartment deaerated cell, with 100 ml of 1 M NaOH and 0.1 M $NaNO_3$ in the working compartment. Compact and porous Cu-Ni RDEs were used for recording cyclic voltammograms and chronoamperometries, compact and porous sheet electrodes (about 3.0 cm^2 of immersed area) for prolonged electrolyses. Analyses of the products were performed by withdrawing 0.1 mL samples from the cathodic compartment with a precision pipette and assessing the products with a Metrohm model 850 Professional IC Ion Chromatograph [38].

3. Results and discussion

3.1. Electrodeposition of porous Cu-Ni on RDE electrodes.

A series of preliminary electrodepositions is performed to identify good operating conditions. The baths used for these preliminary trials are either 0.08 M $CuSO_4$, 0.175 M $NiSO_4$, 0.30 M citrate, or a similar solution containing either 1 M $(NH_4)_2SO_4$ or 2 M NH_4Cl (bath II in Table 1). A benign role of the ammonium ion is indeed reported for deposition of the (porous) single metals, Cu [14] and Ni [16].

With the ammonium-free bath the deposited layer is rather powdery under all the explored deposition conditions. With the ammonium sulphate bath, conversely, it is possible to obtain the desired morphology by acting on the current density, as illustrated in Fig. 1. The deposit obtained with $j_{dep} = -0.3$ A cm^{-2} is globular (Fig. 1a); that obtained with $j_{dep} = -1.0$ A cm^{-2} shows an

Please cite this article in press as: L. Mattarozzi, et al., Hydrogen evolution assisted electrodeposition of porous Cu-Ni alloy electrodes and their use for nitrate reduction in alkali, Electrochim. Acta (2014), http://dx.doi.org/10.1016/j.electacta.2014.04.048

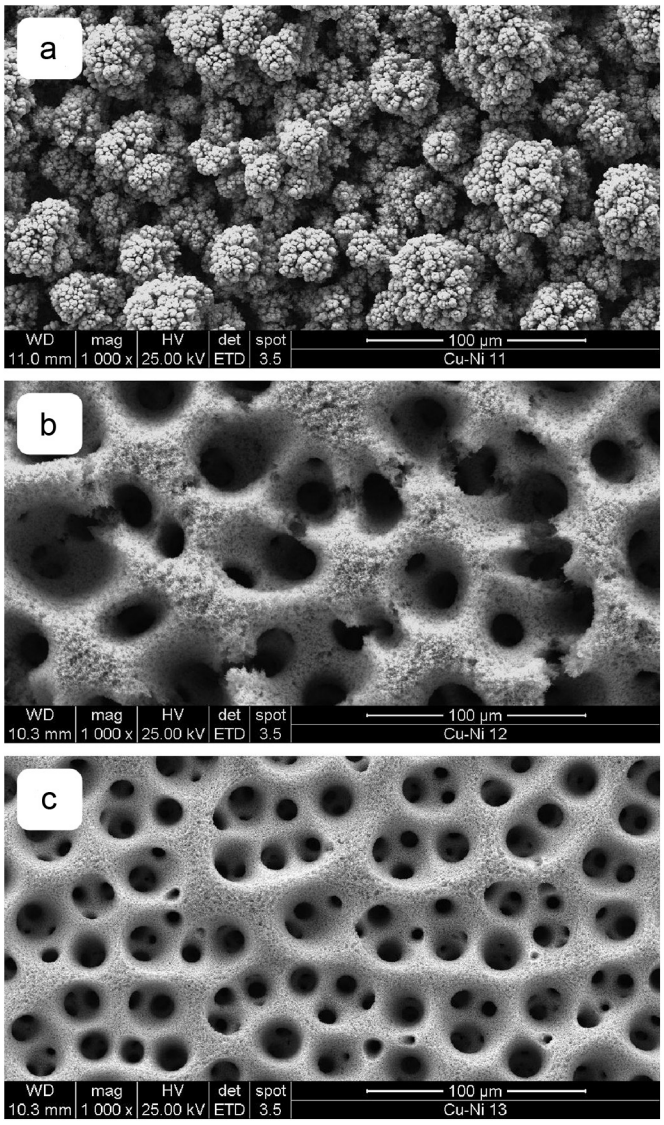

Fig. 1. SEM images of deposits obtained on Nb RDE (2500 min^{-1}) from bath II (Table 1) by galvanostatic polarization (deposition charge 40 C cm^{-2}) at different current densities: a) j_{dep} = -0.3 A cm^{-2} (alloy composition $Cu_{75}Ni_{25}$); b) j_{dep} = -1.0 A cm^{-2} ($Cu_{56}Ni_{44}$); c) j_{dep} = -3.0 A cm^{-2} ($Cu_{52}Ni_{48}$).

irregular, fractured spongy aspect (Fig. 1b); the layer obtained with j_{dep} =-3.0 A cm^{-2} shows a regular spongy material, with a 3D pattern of macropores having diameters in the order of tens of microns (Fig. 1c). Using ammonium chloride, the obtained morphologies are very similar but the copper content is larger and the tendency of the deposit to fracture more pronounced. For this reason only the sulphate bath is used in the following.

The obtained deposits show good adhesion to the substrate and good mechanical resistance, as proved by the regular, essentially flawless structure, despite generation in a rude regime of hydrogen evolution, and the unchanged aspect of the porous layer after prolonged (1 h) operation as RDE at 900 min^{-1} in nitrate reduction (see below), verified by an accurate SEM inspection. Hence, all the subsequent depositions are performed at j_{dep} = -3.0 A cm^{-2}, varying only concentrations of species in the bath. The current density is large but not extreme and under our operating conditions the sort of passivation phenomena termed in the literature "electrode effects" [40–42], involving electrode blanketing by a gas layer, are never observed.

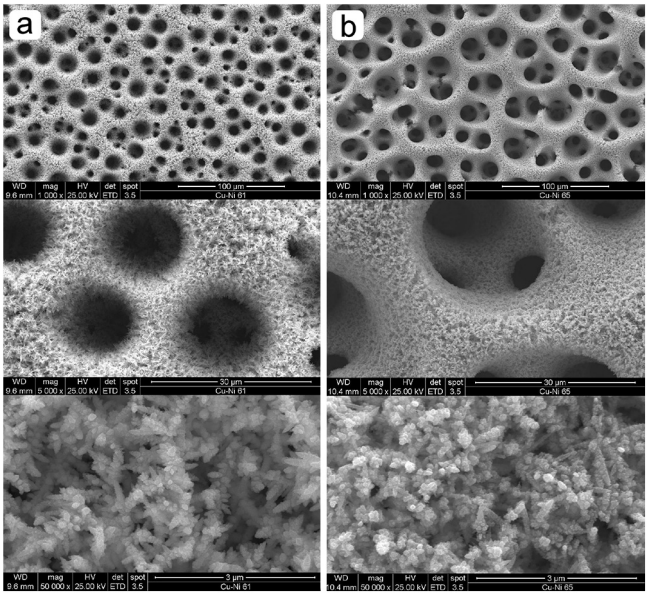

Fig. 2. SEM images of deposits obtained on Nb RDE (2500 min^{-1}), after galvanostatic polarization (deposition charge 40 C cm^{-2}) at j_{dep} = -3.0 A cm^{-2}, in: a) bath I, alloy $Cu_{33}Ni_{67}$; b) bath III, alloy $Cu_{70}Ni_{30}$.

Fig. 2 reports the SEM images of deposits obtained on RDEs (2500 min^{-1}), after galvanostatic polarization at j_{dep} = -3.0 A cm^{-2} (deposition charge 40 C cm^{-2}) in the sulphate solutions I) and III) of Table 1. The images show a rather homogeneous, macroporous 3D structure, with features in the range of tens of microns. The Cu content increases in the series I) to IV), but deposits with Cu content above 70 at% show a tendency to fracture, increasing with the Cu content and rather marked for samples obtained from bath IV.

The high magnification SEM images (Fig. 2, bottom) show that the material consists of a network of small dendrites with typical dimensions below 500 nm. The bimodal porosity, common to all porous metals grown in a similar way [13,14,22,23], originates from the peculiar growth mechanism. The pits with a diameter of tens of microns result from the shaping action exerted by hydrogen bubbles sticking to the electrode, whereas the spongy structure made of needle-like crystals forms under mass transfer conditions. The latter favour limited dendritic growth: the frequent bubbles detachment causes solution renewal, limits the formation of concentration gradients and prevents the formation of long fragile dendrites, typical of metals growth under pure transport control. The resulting metal network is a foam-like structure with a good mechanical resistance. The morphology of the porous alloy deposits obtained on sheet electrodes polarised in a stirred solution is, disregarding a somewhat higher tendency to fracture (Fig. 3a), very similar to those of deposits obtained on RDEs (Fig. 1-2), indicating that the deposition process and the local hydrodynamics are essentially controlled by growth and detachment of hydrogen bubbles.

According to literature ([23] and references therein), growth of spongy-like structures made of dendrites requires specific electrocrystallization properties, namely high exchange current density j_0, low deposition overpotential η and low melting point T_m–properties typical e.g. of Cu. Conversely, formation of the mentioned structures is not expected for metals like Ni, with low exchange current density for deposition j_0, fairly high deposition overpotential η, high melting point T_m, and indeed "porous" Ni deposits [16–19] show an inner cauliflower structure and an outer globular morphology, more dense and compact than that of Fig. 2. Apparently, the presence of Cu creates favourable conditions for formation of spongy binary alloys, even when the second metal is

Please cite this article in press as: L. Mattarozzi, et al., Hydrogen evolution assisted electrodeposition of porous Cu-Ni alloy electrodes and their use for nitrate reduction in alkali, Electrochim. Acta (2014), http://dx.doi.org/10.1016/j.electacta.2014.04.048

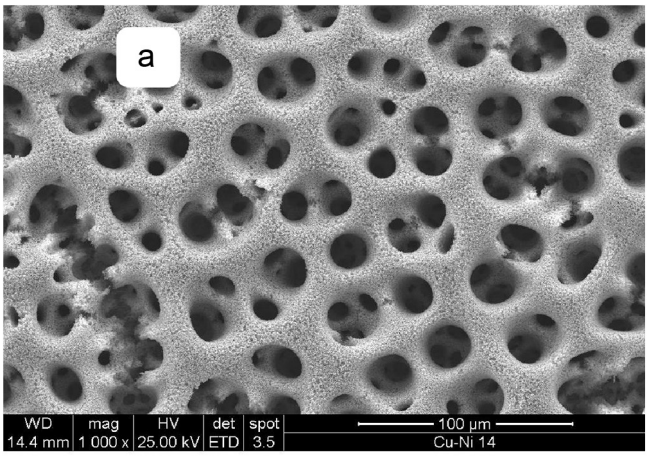

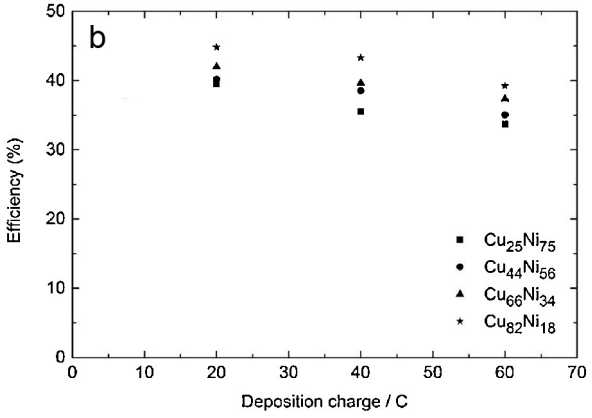

Fig. 3. a) SEM image of the deposit (40 C cm^{-2}) obtained on Nb sheet electrodes (3 cm^2) from bath III, alloy composition $Cu_{66}Ni_{34}$; b) efficiency of alloy deposition, based on estimation of weight increase for deposits obtained from baths I-IV (Table 1), as a function of deposition charge.

not prone to deposit according to this morphology (see e.g. preparation of porous Cu-Ru [27]).

3.2. Characterization of the deposited porous alloy layers.

The composition of some deposited alloys, estimated by EDS over a large area, is summarized in Table 1 for both RDEs and sheet electrodes.

The charge efficiency of alloy deposition has been estimated on sheet electrodes as

$$\text{Eff\%} = \frac{\Delta Q_{dep}}{\Delta Q_{tot}} \times 100 = \frac{2F}{\Delta Q_{tot}} \times \frac{\Delta W_{exp}}{X_{Cu}AW_{Cu} + X_{Ni}AW_{Ni}} \times 100 \quad (1)$$

where: F is the Faraday; ΔQ_{tot} is the total charge passed; ΔQ_{dep} is the charge effectively used for deposition, calculated from the weight increase associated to alloy deposition, ΔW_{exp}, and the atomic fractions X_{Cu} and X_{Ni} of the two metals, estimated by EDS, each multiplied by its corresponding atomic weight AW. Loss of material due to powder formation and/or detachment of small pieces was never appreciable during our short electrolyses, and became significant only for deposition of much thicker alloy layers. The obtained efficiency values, reported in Fig. 3b, are in the range 38-47% for a deposition charge of 20 C cm^{-2} and decrease with film thickening, attaining values in the range 32-40% for a deposition charge of 60 C cm^{-2}. Moreover, for any given deposition charge the estimated efficiency decreases on increasing the Ni content of the deposit. The latter observation is consistent with the higher activity of Ni in hydrogen evolution, as compared to Cu; the decrease in

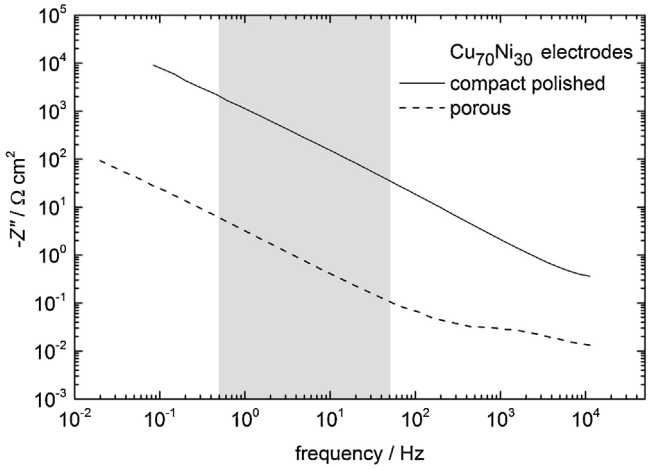

Fig. 4. Impedance response recorded at E = -0.70 V for a porous $Cu_{70}Ni_{30}$ stationary disk electrode (deposition charge 40 C cm^{-2}), and a compact polished electrode of same composition. Bi-logarithmic plots of the dependence of $-Z''$ on frequency, showing very similar slopes (close to -0.88) in the shadowed frequency range.

electrodeposition efficiency with film thickening must also depend on a relative increase of hydrogen evolution, but the reasons are less obvious. Spongy deposits of about 5 mg cm^{-2} obtained with 40 C cm^{-2} show a thickness of 35-40 µm, an apparent density of 1.4 and, considering the compact alloy density (≅ 9), a void volume fraction of 84-85%.

Selected porous Cu-Ni layers deposited on Nb sheets, with EDS composition rather regularly spaced (Table 1), were submitted to XRD analysis. The X-ray diffractograms, reported in a previous paper [39], show alloy peaks located between the corresponding peaks of the single metals, with a linear dependence of the calculated cell parameter on composition, in agreement with the formation of a solid solution respecting Vegard's law. Considering the peak width at half height and using the Scherrer's formula we estimate the typical dimension of crystallites at about 13 nm. However, a certain peak broadening might result from distribution of compositions, leading us to underestimate the real crystallite dimensions. Hence, we looked for further information performing EBSD investigations [4] (not shown) directly at the dendrite scale. The signal is frequently absent or rather blurry, indicating that the crystallite dimensions are typically below instrumental resolution (20 nm). A certain number of spots provides the expected EBSD patterns of a FCC structure, but positions separated by a distance in the order of 50 nm correspond to different reciprocal crystal orientations. On the basis of Scherrer's analysis and EBSD results we can conclude that the material is highly polycrystalline, with crystallite dimensions d typically in the range 10 nm < d < 20 nm and occasionally with d > 20 nm.

EIS spectra were recorded on stationary disk electrodes in 1 M NaOH, at E = -0.70 V, a potential at which the electrode is blocking [38]. The log-log plots of $-Z''$ vs frequency for porous and "compact polished" $Cu_{70}Ni_{30}$ electrodes (Fig. 4) show a CPE behaviour [43], i.e. a linear dependence of $-Z''$ on frequency over at least 2 decades (0.5 Hz to 50 Hz), with a common slope of -0.88. In such cases the capacity cannot be evaluated as $C = [-2\pi f Z'']^{-1}$ at any frequency f. Formulas proposed for the calculation of capacity from CPE parameters [44,45] might allow a sound determination of C only if the reasons for the CPE behaviour were clearly identified [46], which is not the case in the present study. Considering that similar slopes are observed for both alloy morphologies, the roughness factor f_r can be directly estimated as the ratio $f_r \cong Z_c''/Z_p''$ - where Z_c'' and Z_p'' represent the imaginary parts of the impedance of the compact and porous electrode, respectively, measured at the same frequency. In

Please cite this article in press as: L. Mattarozzi, et al., Hydrogen evolution assisted electrodeposition of porous Cu-Ni alloy electrodes and their use for nitrate reduction in alkali, Electrochim. Acta (2014), http://dx.doi.org/10.1016/j.electacta.2014.04.048

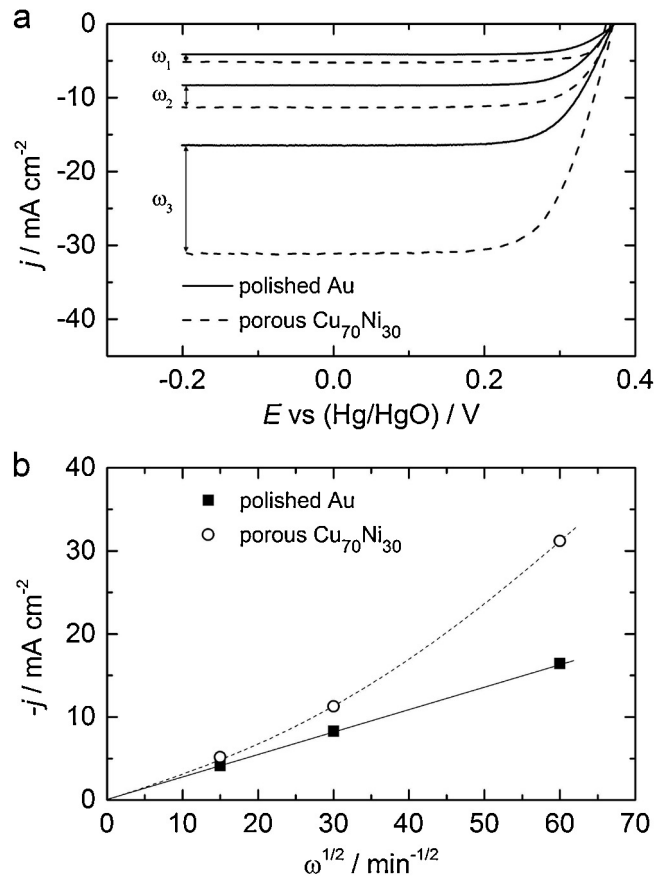

Fig. 5. a) comparison of voltammograms recorded at 10 mV s^{-1} in a solution of 0.020 M $K_3Fe(CN)_6$ and 0.020 M $K_4Fe(CN)_6$ in 1.0 M KOH at a polished Au RDE and a porous $Cu_{70}Ni_{30}$ RDE for different rotation speeds: ω_1 =225 min^{-1}; ω_2 = 900 min^{-1}; ω_3 = 3600 min^{-1}; b) Levich plot of plateau current densities; the dashed line connecting the points relevant to porous $Cu_{70}Ni_{30}$ is merely a guide for the eye.

the frequency range f = 0.5-50 Hz, one finds a rather constant value $f_r \cong 360$. Considering that the polished sample is not ideally smooth, we can take 360 as the minimum roughness factor of the porous electrode. With the same approach, the roughness factor of a compact (not polished) $Cu_{70}Ni_{30}$ electrode was evaluated as $f_r \cong 1.5$: hence, a porous $Cu_{70}Ni_{30}$ electrode has a surface area that is about 240 times that of a compact one.

3.3. *Use as cathode for a kinetically fast reaction. Reduction of ferricyanide in alkali.*

To evaluate the effect of layer morphology on transport, we have performed comparative experiments on a model system, i.e. ferricyanide reduction in alkali, at a smooth mirror-like Au RDE providing a good reference flat surface, and at a porous RDE of composition $Cu_{70}Ni_{30}$, providing very regular morphology and macropores with open structure (Fig. 2). The voltammograms (Fig. 5a) are recorded in a solution of 20 mM $K_3Fe(CN)_6$ and 20 mM $K_4Fe(CN)_6$ in 1.0 M KOH, at different rotation speeds (ω = 225 min^{-1}, 900 min^{-1}, 3600 min^{-1}). The dependence of the current measured at a porous Cu-Ni electrode on ω (Fig. 5b) resembles to those reported in the literature for porous RDEs (PRDE) based on carbon fibre layers [47–49]: in the limit of low rotation rates the dependence tends to Levich relation [50]

$$j_{\lim} = 0.62nFAD_O^{2/3}\nu^{-1/6}\omega^{1/2}C_O \quad (2)$$

but on increasing ω the current exceeds markedly the values established by that relation [48,49]. The quantitative j_{lim}-ω dependence

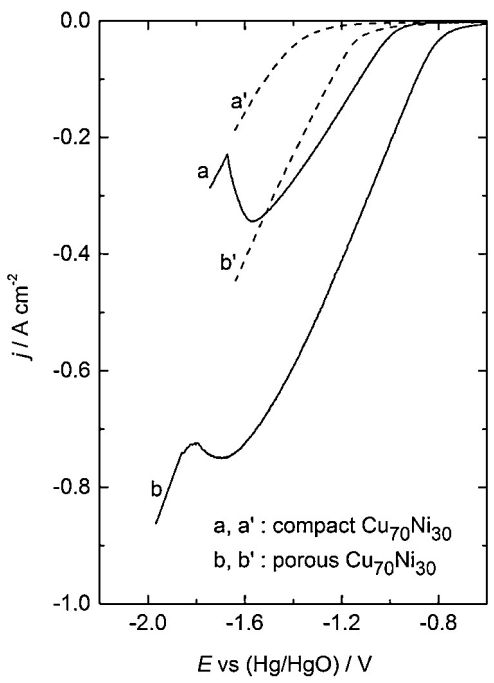

Fig. 6. Voltammograms (20 mV s^{-1}) recorded at a, a') compact and b, b') porous $Cu_{70}Ni_{30}$ RDEs. (900 min^{-1}). Solid curves represent experiments in a solution of 1 M NaOH + 0.1 M $NaNO_3$, dashed curves experiments in 1 M NaOH.

for PRDEs is a complex function of operating parameters including thickness, radius and permeability of the porous layer. However, the limiting situations are conceptually simple: at low rotation rates the current is controlled by reactant diffusion to the outer electrode surface (Levich dependence), but as ω is increased above a critical value, the reaction involves the porous inner volume (electrode perfusion) and the current exceeds the Levich dependence. The deviation from Levich law is smaller in our experiments than in [47–49] due to the low thickness/radius ratio of the Cu-Ni porous electrodes and the narrower explored ω range.

The Levich dependence implies a diffusion layer thickness $\delta_0 = 1.61D_O^{1/3}\omega^{-1/2}\nu^{1/6}$; δ_0 values of 25.4 μm, 12.7 μm and 6.35 μm may be calculated for ω = 225 min^{-1}, 900 min^{-1}, and 3600 min^{-1}, respectively, using ν = 0.01 cm^2 s^{-1} [50] and D_O = 0.45·10^{-5} cm^2 s^{-1} (relevant to 2 M NaOH, [51]). These values are comparable to, or lower than, the typical dimensions of pores mouth and so an increased accessibility of the inner pore surface may enhance the current even when the flow rate of the electrolyte through the porous electrode is not very significant. Current enhancement due to onset of turbulence is unlikely to occur [48].

3.4. *Voltammetric investigations of the reduction of nitrate ions in alkali.*

We have tested the Cu-Ni electrodes as cathodes for reduction of nitrate in 1.0 M NaOH, an alkaline medium that may be considered representative of some industrial waste solutions [29,30], but also of the treatment of polluted neutral wastewaters, since the reduction processes

$$NO_3^- + H_2O + 2e^- \rightarrow NO_2^- + 2OH^- \quad (3)$$

$$NO_2^- + 5H_2O + 6e^- \rightarrow NH_3 + 7OH^- \quad (4)$$

$$NO_3^- + 6H_2O + 8e^- \rightarrow NH_3 + 9OH^- \quad (5)$$

produce a local alkalinisation of the solution.

Fig. 6 shows the voltammograms recorded at $Cu_{70}Ni_{30}$ RDEs (900 min^{-1}) in 1.0 M NaOH + 0.1 M $NaNO_3$ (solid curves) and 1.0 M

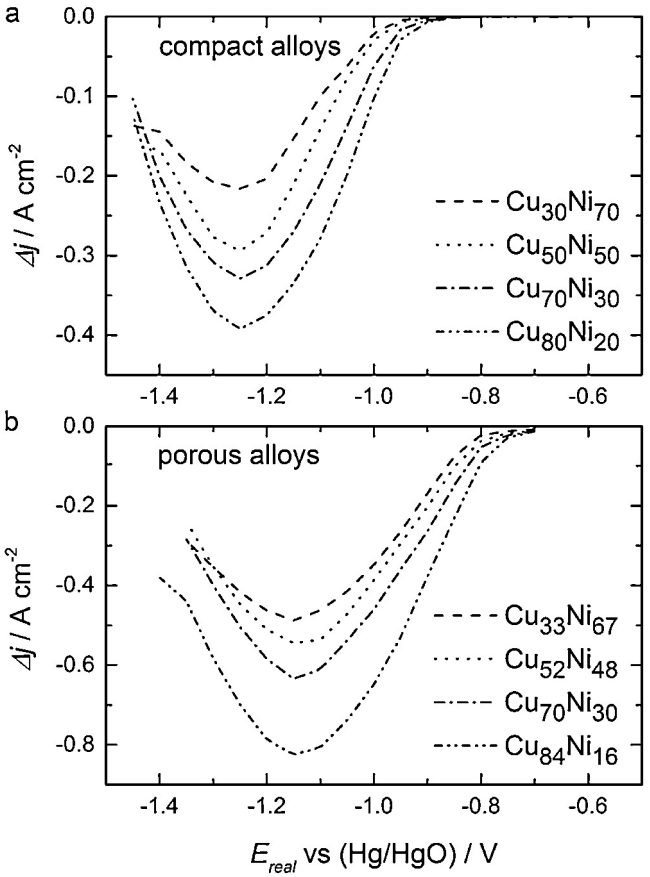

Fig. 7. Voltammograms (20 mV s^{-1}) recorded at compact and porous RDEs (900 min^{-1}) of indicated compositions, in a solution of 1 M NaOH + 0.1 M $NaNO_3$, after correction for IR drop and subtraction of hydrogen evolution current (see text).

NaOH (dashed curves). The voltammogram of nitrate reduction at compact electrodes (curve a) shows a large current peak that does not attain a diffusion plateau, as already observed in a previous publication for lower nitrate concentrations [38]. The experiment recorded at the porous electrode (curve b) shows a shift of current onset towards less negative potentials and a much larger current maximum, which appears located at more negative potentials. It must be considered that the two electrodes display a different ability to perform the hydrogen evolution reaction (curves a', b'), and that *IR* drop distorts the curves to different extents.

Hence, in Fig. 7 we compare also the plots of the net current of nitrate reduction Δj, calculated by subtracting the current density measured, at each (real) potential, in 1 M NaOH from that measured in 1.0 M NaOH + 0.1 M $NaNO_3$. We have first corrected the curves for the *IR* drop, then subtracted the curves point-by-point at (corresponding) real electrode potentials. These corrected curves, relevant to all the 4 compositions reported in Table 1 for RDEs, show that at the porous electrodes the foot of the voltammetric *j-E* curve is displaced by almost 200 mV towards less negative potentials, with respect to the compact electrodes. However, if the current densities measured at porous and compact electrodes are referred to the estimated true surface areas (ca. 240 times larger for the former, see section 3.2), the *j-E* curves tend to overlap in the potential range where the nitrate reduction reaction is expected to be under pure kinetic control. This indicates that the shift in the current onset is not due to real electrocatalytic effects but rather to geometric factors, that may be nonetheless valuable in applications [52]. The curves in Fig. 7 also show that the peak currents measured at porous electrodes are twice larger than those observed at a compact electrode of very similar composition, the peak potentials

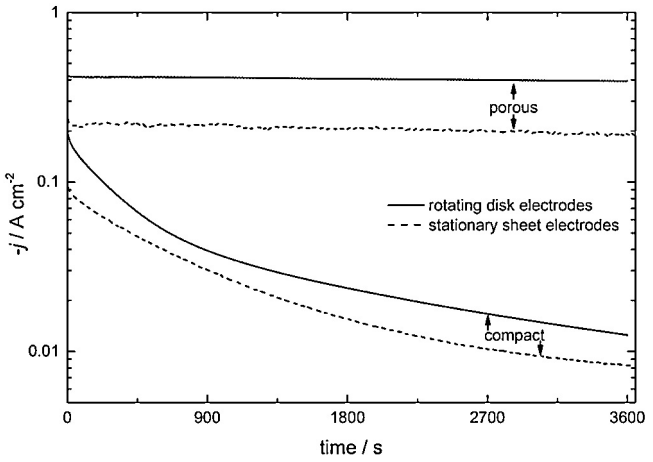

Fig. 8. Chronoamperometric curves recorded in 1 M NaOH + 0.1 M $NaNO_3$, applied potential *E* = -1.20 V vs Hg/HgO, at compact and porous $Cu_{70}Ni_{30}$ electrodes: RDEs rotated at 900 min^{-1} (solid lines); stationary sheet electrodes, stirred solution (dashed lines).

being less negative by ca. 100 mV. Since the size of the peak is controlled by various factors, including nitrate ion mass transport, adsorption of reaction intermediates and H atoms, and possibly pore filling by gaseous H_2, the peak current is not expected to scale with the true surface area. One may note that the peak current enhancement factor (ca. 2) is larger than that measured with the diffusion controlled ferricyanide reduction at the same rotation rate (ca. 1.35, compare Fig. 5).

3.5. Constant potential electrolyses and analysis of reaction products.

Chronoamperometric experiments have been recorded in 0.1 M $NaNO_3$ + 1 M NaOH at E = -1.20 V with compact and porous $Cu_{70}Ni_{30}$ RDEs, a composition offering a good compromise between catalytic efficiency (larger at large Cu contents [38]) and mechanical stability (lower for Cu contents exceeding 70 at%). Results reported in Fig. 8 (solid lines) show that the initial current (t = 0) is about twice larger at the porous electrode, in basic agreement with voltammetric data. However, a major difference in time evolution is observed: during the first hour of polarisation, the current decays substantially at the compact electrode, and remains almost constant at the porous electrode, with a minor decay basically reflecting the decrease of concentration of the active species in solution. After 1 h of polarisation the current observed at the porous electrode is ca. 30 times larger than that observed at compact electrodes. The experiments recorded at the two sheet electrodes (3 cm^2), compact and porous (Fig. 8, dashed lines), show a lower current density due to the less efficient mass transport regime, but analogous *j*-time dependencies.

Results of prolonged electrolyses are summarized in Table 2, reporting the analytical data and some basic elaborations. In particular: a) the selectivity for NH_3 production, defined as the ratio $[NH_3]_t/([NO_3^-]_{in}-[NO_3^-]_t)$, where $[NH_3]_t$, $[NO_3^-]_t$ indicate the concentrations at time t and $[NO_3^-]_{in}$ the initial concentration (0.1 M) at t = 0; b) the current efficiency for production of NO_2^- and NH_3, estimated as the ratio % between the charge used to generate the given species and the total charge, and "other", calculated as the complement to 100%. The last term includes production of H_2 (according to literature, the dominant side product) and possible minor amounts of N_2. The total final concentration of nitrogen-containing species is regularly below the initial NO_3^- concentration (100 mM), indicating that a few % of the product is lost undetected. Considering that the

Table 2
Products of electrolysis of 100 ml of alkaline solutions (1 M NaOH) containing 0.1 M NO_3^-. Alloy sheet electrodes, surface of 3 cm^2, applied potential E = -1.2 V.

Electrode material	Time (h)	Charge (C)	$[NO_3^-]_t \cdot 10^{-3}$ M	$[NO_2^-]_t \cdot 10^{-3}$ M	$[NH_3]_t \cdot 10^{-3}$ M	a) Selectivity to NH_3 (%)	b) Current efficiency (%) for production of		
							NO_2^-	NH_3	Other
Cu70Ni30 compact	0	0	100.0	0	0	-	-	-	-
	2	329.5	94.2	2.4	3.4	58.3	14.1	79.2	6.6
	4	452.2	92.2	3.2	4.6	58.9	13.7	78.7	7.5
	6	562.6	90.2	3.9	5.7	58.2	13.5	78.5	8.0
	8	672	88.9	4.2	7.0	62.7	12.1	79.8	8.1
Cu70Ni30 porous	0	0	100.0	0	0	-	-	-	-
	1	1846	72.8	2.4	23.2	85.4	2.5	97.2	0.3
	2	3340	53.1	3.7	41.9	89.4	2.1	96.9	1.0
	3	4475	38.7	3.8	56.6	92.3	1.6	97.6	0.8
	4	5305	28.4	3.4	67.2	93.8	1.2	97.8	0.9
	6	6296	17.4	2.5	78.1	94.6	0.8	95.8	3.5
	8	6826	13.2	1.5	83.2	95.9	0.4	94.1	5.5

a) Selectivity: moles of ammonia produced over moles of original oxyanion disappeared (see text)
b) Current Efficiency: charge used to generate the given product as a % of total charge

deficiency of total nitrogen correlates with the presence of ammonia in solution, at least part of it may be attributed to ammonia losses during electrolysis (from a non-tight cell) and sampling operations. However, some production of (undetected) nitrogen cannot be ruled out. It must be noticed that the rate of disappearance of nitrate (Table 2) is larger by factors of 7-9 at the porous electrode in comparison with the compact one: this marked improvement of performances results from the lower deactivation of the porous electrode that is shown by the chronoamperometric curves in Fig. 8.

Hence, in comparison with the compact alloy the porous material of equivalent composition offers better performances in terms of: i) faster elimination of NO_3^-; ii) limited production of NO_2^-; iii) high selectivity towards formation of a main product (NH_3), with possible minor production of gaseous N_2. The good stability of electrode performances (Fig. 8) allows fast and drastic reduction of the nitrate concentration in a single treatment (Table 2).

To clarify the reasons of the superior current stability at the porous electrodes we have performed CVs (not reported) in 1 M NaOH at compact and porous electrodes i) freshly deposited and ii) submitted to 1 h polarization. The basic voltammetric peaks are similar at the fresh and aged electrodes, and no remarkable additional peak is detected, indicating that the current decay observed at the compact electrode during nitrate reduction isn't primarily due to deposition of impurities from the alkaline solution. Some observed modifications of the pattern (relative peak heights of the systems relevant to Cu and Ni) provide little information. In the absence of firm evidence, the "passivation phenomena" observed during nitrate reduction on compact electrodes may be tentatively attributed to inactivation of catalytic surface sites, due e.g. to adsorption of elusive, N-containing reaction intermediates [35]. Since the ratio of true surface area of the porous $Cu_{70}Ni_{30}$ electrode to that of the compact is about 240, and the ratio of the corresponding reduction currents varies from 2 to 25-30 during 1-hour electrolyses, the observed difference in deactivation rates may be explained assuming that the production of "poisoning" species is proportional to current, and that a much smaller surface fraction would be inactivated at the large area porous alloy than at the compact material.

4. Conclusions

Porous Cu-Ni alloys with a fairly large range of compositions can be electrodeposited from citrate baths containing the two metal ions and ammonium sulphate, under application of large reduction current densities (-3 A cm^{-2}). SEM images show a bimodal porosity: macropores with tens of microns diameter, due to the shaping action of gas bubbles evolving during current application, and a spongy structure appearing as a network of tiny polycristalline dendrites.

Use of the spongy alloys as cathodes shows a significant current increase for reactions under pure mass transport control, in agreement with literature studies on porous rotating disc electrodes [47–49]. The porous alloys show better activity and stability of performance in the reduction of nitrate, in comparison with the compact alloys, especially at moderately negative potentials (E = -1.20 V vs Hg/HgO). Both improvements must be ascribed mainly to their porous structure and morphology: (i) the current density, referred to the *geometric* area, is enhanced by surface roughness and electrode perfusion; (ii) the rate of electrode inactivation, ascribed to poisoning intermediates, is lower due to the much larger *real* surface area. The porous electrodes show also better selectivity, as they produce almost exclusively a single species, NH_3, which may be oxidized to harmless N_2 in further steps of the remediation treatment.

References

[1] M. Lai, D.J. Riley, Templated electrosynthesis of nanomaterials and porous structures, Journal of Colloid and Interface Science 323 (2008) 203–212.
[2] C. Schönenberger, B.M.I. van der Zande, L.G.J. Fokkink, M. Henny, C. Schmid, M. Krüger, A. Bachtold, R. Huber, H. Birk, U. Staufer, Template synthesis of nanowires in porous polycarbonate membranes: electrochemistry and morphology, Journal of Physical Chemistry B (1997) 5497–5505.
[3] Y. Konishi, M. Motoyama, H. Matsushima, Y. Fukunaka, R. Ishii, Y. Ito, Electrodeposition of Cu nanowire arrays with a template, Journal of Electroanalytical Chemistry 559 (2003) 149–153.
[4] A. Gambirasi, S. Cattarin, M. Musiani, L. Vázquez-Gómez, E. Verlato, Direct electrodeposition of metal nanowires on electrode surface, Electrochimica Acta 56 (2011) 8582–8588.
[5] H. Pan, B. Liu, J. Yi, C. Poh, S. Lim, J. Ding, Y. Feng, C.H.A. Huan, J. Lin, Growth of single-crystalline Ni and Co nanowires via electrochemical deposition and their magnetic properties, Journal of Physical Chemistry B 109 (2005) 3094–3098.
[6] R. Inguanta, S. Piazza, C. Sunseri, Influence of the electrical parameters on the fabrication of copper nanowires into anodic alumina templates, Applied Surface Science 255 (2009) 8816–8823.
[7] P.N. Bartlett, J.J. Baumberg, P.R. Birkin, M.A. Ghanem, M.C. Netti, Highly ordered macroporous gold and platinum films formed by electrochemical deposition through templates assembled from submicron diameter monodisperse polystyrene spheres, Chemistry of Materials 14 (2002) 2199–2208.
[8] M.E. Abdelsalam, P.N. Bartlett, J.J. Baumberg, S. Coyle, Preparation of arrays of isolated spherical cavities by self-assembly of polystyrene spheres on self-assembled pre-patterned macroporous films, Advanced Materials 16 (2004) 90–93.
[9] R. Szamocki, A. Velichko, C. Holzapfel, F. Mucklich, S. Ravaine, P. Garrigue, N. Sojic, R. Hempelmann, A. Kuhn, Macroporous ultramicroelectrodes for improved electroanalytical measurements, Analytical Chemistry 79 (2007) 533–539.
[10] M. Heim, S. Reculusa, S. Ravaine, A. Kuhn, Engineering of complex macroporous materials through controlled electrodeposition in colloidal superstructures, Advanced Materials 22 (2012) 538–545.

Please cite this article in press as: L. Mattarozzi, et al., Hydrogen evolution assisted electrodeposition of porous Cu-Ni alloy electrodes and their use for nitrate reduction in alkali, Electrochim. Acta (2014), http://dx.doi.org/10.1016/j.electacta.2014.04.048

[11] Y. Li, W.-Z. Jia, Y.-Y. Song, X.-H. Xia, Superhydrophobicity of 3D porous copper films prepared using the hydrogen bubble dynamic template, Chemistry of Materials 19 (2007) 5758–5764.
[12] H.-C. Shin, J. Dong, M. Liu, Nanoporous structures prepared by an electrochemical deposition process, Advanced Materials 15 (2003) 1610–1614.
[13] H.-C. Shin, M. Liu, Copper foam structures with highly porous nanostructured walls, Chemistry of Materials 16 (2004) 5460–5464.
[14] D.H. Nam, R.H. Kim, D.W. Han, J.H. Kim, H.S. Kwon, Effects of $(NH_4)_2SO_4$ and BTA on the nanostructure of copper foam prepared by electrodeposition, Electrochimica Acta 56 (2011) 9397–9405.
[15] N.D. Nikolić, and K.I. Popov, in Modern Aspects of Electrochemistry, Vol. 48, S.S. Djokić, Editor, p. 1, Springer, New York (2010), pp. 1-70.
[16] C.A. Marozzi, A.C. Chialvo, Development of electrode morphologies of interest in electrocatalysis. Part 1: Electrodeposited porous nickel electrodes, Electrochimica Acta 45 (2000) 2111–2120.
[17] F. Huet, M. Musiani, R.P. Nogueira, Oxygen evolution on electrodes of different roughness: an electrochemical noise study, Journal of Solid State Electrochemistry 8 (2004) 786–793.
[18] L. Vázquez-Gómez, S. Cattarin, P. Guerriero, M. Musiani, Hydrogen evolution on porous Ni cathodes modified by spontaneous deposition of Ru or Ir, Electrochimica Acta 53 (2008) 8310–8318.
[19] L. Vázquez-Gómez, S. Cattarin, R. Gerbasi, P. Guerriero, M. Musiani, Activation of porous Ni cathodes towards hydrogen evolution by electrodeposition of Ir nuclei, Journal of Applied Electrochemistry 39 (2009) 2165–2172.
[20] L. Vázquez-Gómez, E. Verlato, S. Cattarin, N. Comisso, P. Guerriero, M. Musiani, Electrodeposition of porous Co Layers and their conversion to electrocatalysts for methanol oxidation by spontaneous deposition of Pd, Electrochimica Acta 56 (2011) 2237–2245.
[21] S. Cherevko, X. Xing, C.-H. Chung, Electrodeposition of three-dimensional porous silver foams, Electrochemistry Communications 12 (2010) 467–470.
[22] S. Cherevko, C.-H. Chung, Impact of key deposition parameters on the morphology of silver foams prepared by dynamic hydrogen template deposition, Electrochimica Acta 55 (2010) 6383–6390.
[23] S. Cherevko, C.-H. Chung, Direct electrodeposition of nanoporous gold with controlled multimodal pore size distribution, Electrochemistry Communications 13 (2011) 16–19.
[24] H.-C. Shin, M. Liu, Three-Dimensional Porous Copper-Tin Alloy Electrodes for Rechargeable Lithium Batteries, Advanced Functional Materials 15 (2005) 582–586.
[25] S. Cherevko, N. Kulyk, C.-H. Chung, Nanoporous Pt@Au_xCu_{100-x} by hydrogen evolution assisted electrodeposition of Au_xCu_{100-x} and galvanic replacement of Cu with Pt: electrocatalytic properties, Langmuir 28 (2012) 3306–3315.
[26] M.-G. Jeong, K. Zhuo, S. Cherevko, C.-H. Chung, Formation of nanoporous nickel oxides for supercapacitors prepared by electrodeposition with hydrogen evolution reaction and electrochemical dealloying, Korean Journal of Chemical Engineering 29 (2012) 1802–1805.
[27] M.-G. Jeong, K. Zhuo, S. Cherevko, W.-J. Kim, C.-H. Chung, Facile preparation of three-dimensional porous hydrous ruthenium oxide electrode for supercapacitors, Journal of Power ources 244 (2013) 806–811.
[28] C. Milhano, D. Pletcher, The electrochemistry and electrochemical technology of nitrate, in: R.E. White (Ed.), Modern Aspects of Electrochemistry, Volume 45, Springer, Dordrecht, 2009, pp. 1–61.
[29] V. Rosca, M. Duca, M.T. de Groot, M.T.M. Koper, Nitrogen cycle electrocatalysis, Chemical Reviews 109 (2009) 2209–2244.
[30] H. Li, D.H. Robertson, J.Q. Chambers, D.T. Hobbs, Electrochemical reduction of nitrate and nitrite in concentrated sodium hydroxide at platinum and nickel electrodes, Journal of the Electrochemical Society 135 (1988) 1154–1158.
[31] K. Bouzek, M. Paidar, A. Sadilkova, H. Bergmann, Electrochemical reduction of nitrate in weakly alkaline solutions, Journal of Applied Electrochemistry 31 (2001) 1185–1193.
[32] S. Cattarin, Electrochemical reduction of nitrogen oxyanions in 1 M sodium hydroxide solutions at silver, copper and $CuInSe_2$ electrodes, Journal of Applied Electrochemistry 22 (1992) 1077–1081.
[33] B.K. Simpson, D.C. Johnson, Electrocatalysis of nitrate reduction at copper-nickel alloy electrodes in acidic media, Electroanalysis 16 (2004) 532–538.
[34] C. Milhano, D. Pletcher, The electrodeposition and electrocatalytic properties of copper-palladium alloys, Journal of Electroanalytical Chemistry 614 (2008) 24–30.
[35] D. Reyter, D. Bélanger, L. Roué, Study of the electroreduction of nitrate on copper in alkaline solutions, Electrochimica Acta 53 (2008) 5977–5984.
[36] N. Comisso, S. Cattarin, S. Fiameni, R. Gerbasi, L. Mattarozzi, M. Musiani, L. Vázquez-Gómez, E. Verlato, Electrodeposition of Cu-Rh alloys and their use as cathodes for nitrate reduction, Electrochemistry Communications 25 (2012) 91–93.
[37] E. Verlato, S. Cattarin, N. Comisso, P. Guerriero, L. Mattarozzi, M. Musiani, L. Vázquez-Gómez, Reduction of nitrate ions at Rh-modified Ni foam electrodes, Electrocatalysis 4 (2013) 203–211.
[38] L. Mattarozzi, S. Cattarin, N. Comisso, P. Guerriero, M. Musiani, L. Vázquez-Gómez, E. Verlato, Electrochemical reduction of nitrate and nitrite in alkaline media at CuNi alloy electrodes, Electrochimica Acta 89 (2013) 488–496.
[39] L. Mattarozzi, S. Cattarin, N. Comisso, R. Gerbasi, P. Guerriero, M. Musiani, L. Vázquez-Gómez, E. Verlato, Electrodeposition of Cu-Ni alloy electrodes with bimodal porosity and their use for nitrate reduction, ECS Electrochemistry Letters 2 (2013) D58–D60.
[40] R. Wüthrich, H. Bleuler, A model for electrode effects using percolation theory, Electrochimica Acta 1547-1554.
[41] R. Wüthrich, Ch. Comninellis, H. Bleuler, Bubble evolution on vertical electrodes under extreme current densities, Electrochimica Acta 50 (2005) 5242–5246.
[42] H. Vogt, R.J. Balzer, The bubble coverage of gas-evolving electrodes in stagnant electrolytes, Electrochimica Acta 50 (2005) 2073–2079.
[43] M.E. Orazem, B. Tribollet, Electrochemical Impedance Spectroscopy, J. Wiley & Sons, Hoboken (NJ), 2008, p. 233.
[44] G.J. Brug, A.L.G. Van Den Eeden, M. Sluyters-Rehbach, J.H. Sluyters, The analysis of electrode impedances complicated by the presence of a constant phase element, Journal of Electroanalytical Chemistry 176 (1984) 275–295.
[45] C.H. Hsu, F. Mansfeld, Concerning the conversion of the constant phase element parameter Y0 into a capacitance, Corrosion 57 (2001) 747–748.
[46] B. Hirschorn, M.E. Orazem, B. Tribollet, V. Vivier, I. Frateur, M. Musiani, Determination of effective capacitance and film thickness from constant-phase-element parameters, Electrochim. Acta 55 (2010) 6218–6227.
[47] W.J. Blaedel, J. Wang, Rotated porous carbon disk electrode, Analytical Chemistry 52 (1980) 76–80.
[48] R.T. Bonnecaze, N. Mano, B. Nam, A. Heller, On the behavior of the porous rotating disk electrode, Journal of the Electrochemical Society 154 (2007) F44–F47.
[49] B. Nam, R.T. Bonnecaze, Analitic models of the infinite porous rotating disk electrode, Journal of the Electrochemical Society 154 (2007) F191–F197.
[50] A.J. Bard, L.R. Faulkner, Electrochemical Methods: Fundamentals and Applications, J. Wiley & Sons, New York, 1980, p. 289.
[51] R.N. Adams, Electrochemistry at Solid Electrodes, Marcel Dekker, New York, 1969, p. 220.
[52] S. Trasatti, Electrocatalysis: understanding the success of DSA, Electrochimica Acta 45 (2000) 2377–2385.

Please cite this article in press as: L. Mattarozzi, et al., Hydrogen evolution assisted electrodeposition of porous Cu-Ni alloy electrodes and their use for nitrate reduction in alkali, Electrochim. Acta (2014), http://dx.doi.org/10.1016/j.electacta.2014.04.048